Journal of the Mechanical Behavior of Biomedical Materials 88 (2018) 346–351

Contents lists available at ScienceDirect

Journal of the Mechanical Behavior of Biomedical Materials

journal homepage: www.elsevier.com/locate/jmbbm

Design of a surrogate for evaluation of methods to predict bone bending stiffness

Caitlyn J. Collins*,[1], Matthew Boyer, Thomas D. Crenshaw, Heidi-Lynn Ploeg

Department of Mechanical Engineering, University of Wisconsin-Madison, 3047 Mechanical Engineering Building, 1513 University Avenue, Madison, WI 53706, United States

A B S T R A C T

The high incidence of osteoporosis and related fractures demands for the use and development of methods capable of detecting changes in bone mechanical properties. The most common clinical and laboratory methods used to detect changes in bone mechanical properties, such as stiffness, strength, or flexural rigidity, include: mechanical testing, medical imaging, medical image-based analytical calculations, and medical image-based finite element analysis. However, the innate complexity of bone makes validation of the results from each method difficult. The current study presents the design, fabrication, and functional testing of a bi-material and computed tomography scan compatible bone-surrogate which provides consistent reproducible mechanical properties for methodological evaluation of experimental, analytical, and computational bone bending stiffness prediction methods.

1. Introduction

In 2014, the National Osteoporosis Foundation reported that over half of the total adult population of the United States over the age of 50 suffered from osteoporosis or low bone mass (Wright et al., 2014). Osteoporotic related fracture is associated with an increased risk of patient morbidity. Despite the severe consequences of osteoporotic related fracture, many patients go undiagnosed until their first fracture.

Due to the limited availability and restrictions associated with the use of human specimens in biomechanics research, many studies use animal models in preclinical studies. Animal models, both large and small, are commonly used to investigate the effect of osteoporosis (Dias et al., 2018; Heiss et al., 2017), fracture healing (Decker et al., 2014), orthopaedic implants (Pearce et al., 2007), diet (Aiyangar et al., 2010; Crenshaw et al., 1981), etc. on the biomechanics of bone. Large animal models such as the sheep, goat, and pig, combined, make up roughly 18% of animal studies focused on bone fracture and 19% on osteoporosis (Martini et al., 2001). Large animal models are particularly relevant for the understanding of human bone because of their more comparable sized skeletons and bone metabolism as opposed to small animal models like the mouse or rat.

The most common clinical and laboratory methods used to detect changes in bone mechanical properties, such as stiffness, strength, or flexural rigidity, include: mechanical testing, medical imaging, medical image-based analytical calculations, and medical image-based finite element analysis. Although the majority of these methods can be used to measure bone mechanical properties, the innate complexity of bone makes validation of bone stiffness prediction methods difficult (Cristofolini et al., 1996; Heiner, 2008). Therefore, a common surrogate is needed to quantify methodological errors across imaging, testing, analytical, and finite element (FE) methods. The objective of this study was to design and fabricate a bi-material surrogate which is computed tomography (CT) scan-compatible in order to provide consistent reproducible mechanical properties for methodological evaluation of experimental, analytical, and computational bone bending stiffness prediction methods. To meet this objective the following steps were taken:

1. Concept Design: Define geometric parameters.
2. Configuration Design: Design custom components and select and test off-the-shelf materials for surrogate.
3. Fabricate and evaluate functional bone surrogate prototype

2. Materials and methods

2.1. Bone surrogate concept design

A porcine femur was used to determine the product design specifications (PDS) of the bone surrogate; however, the PDS could easily be adapted to generate a bone surrogate for a long bone from a different animal model. Functional and size requirements were set such that the total envelope of the surrogate should not exceed 40 mm x 30 mm

* Corresponding author.
E-mail addresses: caitlyn.collins@uwalumni.com (C.J. Collins), tdcrensh@wisc.edu (T.D. Crenshaw), heidi.ploeg@queensu.ca (H.-L. Ploeg).
[1] Present address: Institute for Lightweight Design and Structural Biomechanics, TU Wien, Getreidemarkt 9, BE 0105, 1060 Vienna, Austria.

https://doi.org/10.1016/j.jmbbm.2018.08.046
Received 21 January 2018; Received in revised form 22 May 2018; Accepted 28 August 2018
Available online 30 August 2018

Nomenclature

AC	acetyl copolymer
a	length of the moment arm from the upper to lower support, 12.7 mm
b_b	width of the four-point bending test specimens, mm
CSA_c	cross-sectional area of the compression test specimens, mm^2
CSA_t	cross-sectional area of the tensile test specimens, mm^2
CT	computed tomography
D	support diameter, 0.5 mm
DICOM	Digital Imaging and Communications in Medicine
E_b	elastic bending modulus, MPa; $\left(\frac{a(3Lx-3x^2-a^2)K_b}{12I}\right)$
E_c	elastic compressive modulus, MPa; $\left(K_c\frac{h_c}{CSA_c}\right)$
E_t	elastic tensile modulus, MPa; $\left(K_t\frac{L_t}{CSA_t}\right)$
EI_{eff}	effective flexural rigidity, Nmm^2; $\left(\frac{a(3Lx-3x^2-a^2)K_s}{12}\right)$
$EI_{eff,adj}$	adjusted effective flexural rigidity, Nmm^2; $\left(\frac{a(3Lx-3x^2-a^2)K_s}{12}\right)$
EI_{Goal}	target flexural rigidity, 1–2 × 10^8 Nmm^2
EI_x	flexural rigidity about the x-axis, Nmm^2; $\left(E_{b,AC}\left[\frac{wh^3}{12}+\left(\frac{E_{b,HDPU}}{E_{b,AC}}-1\right)\left(\frac{\pi r^4}{4}\right)\right]\right)$
EI_y	flexural rigidity about the y-axis, Nmm^2; $\left(E_{b,AC}\left[\frac{w^3h}{12}+\left(\frac{E_{b,HDPU}}{E_{b,AC}}-1\right)\left(\frac{\pi r^4}{4}\right)\right]\right)$
E_1	elastic modulus of the steel support (compressive), MPa
E_2	elastic modulus of the AC shell (compressive), MPa
F	force, N
$\bar{F}$	applied force per unit length, N/mm
FE	finite element
HDPU	high density polyurethane foam
HU	Hounsfield unit
h	height, mm
h_b	height of the four-point bending test specimens, mm
h_c	height of the compression test specimens, mm
I	second moment of area about the bending axis, mm^4; $\left(\frac{b_b h_b^3}{12}\right)$
K	stiffness, N/mm; $\left(\frac{F}{\delta}\right)$
L	length of the lower support span, 50.8 mm
L_t	gauge length of the tensile test specimens, ~ 50 mm
m	sample mass, g
PDS	product design specifications
R	radius, mm
V	sample volume, cm^3
w	width, mm
x	position at which displacements were measured, mm
y	local deformation, mm; $\left(\bar{F}\left(\frac{1-\nu_1}{\pi E_1}+\frac{1-\nu_2}{\pi E_2}\right)\left[1+\ln\left\{\frac{8\left(\frac{w}{2}\right)^2}{\left(\frac{1-\nu_1}{\pi E_1}+\frac{1-\nu_2}{\pi E_2}\right)\bar{F}D}\right\}\right]\right)$
δ	displacement, mm
δ_{adj}	adjusted displacement, mm; (δ-2y)
ρ	density, g/cm^3; $\left(\frac{m}{V}\right)$
ν_1	Poisson's ratio of the steel supports
ν_2	Poisson's ratio of the AC shell

x 150 mm in width (w), height (h), or length in order to mimic porcine femur geometry (Crenshaw et al., 1981). The geometric features of the surrogate should be simple to fabricate using standard machine shop equipment. Reported values of porcine femur flexural rigidity under four-point bending test conditions vary widely due to differences in diet, age, and sex (Aiyangar et al., 2010; Crenshaw et al., 1981). Therefore, the final dimensions of the bi-material surrogate should yield a flexural rigidity between 1 and 2 × 10^8 Nmm^2 (EI_{Goal}) to represent the stiffest four-point bending flexural rigidity found within the literature (Aiyangar et al., 2010). For comparison, the flexural rigidity of a sheep femur has been reported as 1 × 10^8 Nmm^2 (Bramer et al., 1998), near the low end of the range found for the pig femur, while the flexural rigidity of the human femur has been reported to range from 2.7 to 3.7 × 10^8 Nmm^2 depending on the direction of the applied bending moment (Cristofolini et al., 1996; Heiner, 2008).

The surrogate materials should be selected from readily available homogeneous stock materials. The two materials selected should have different densities in order to act as density calibration phantoms for medical image-based analysis methods. Both materials should be durable, sterilizable, and non-metallic in order for the surrogate to withstand repeated handling and to be permitted in clinical CT scanners. All selected materials must be non-toxic to prevent release of dangerous byproducts during the machining process.

2.2. Bone surrogate configuration design

To reflect the natural geometry of a porcine femur diaphysis, the surrogate was designed with a stiff outer shell and a more compliant inner core. A rectangular shell cross section was selected to provide distinct h and w dimensions, and to resist rotation during bending mechanical testing. A cylindrical core was selected for ease of machining. Based on the above PDS, stock acetyl co-polymer (AC) and 40 lb/ft^3, Grade 40, high-density polyurethane foam (HDPU) were selected for the shell and core, respectively.

Material testing blanks of AC and HDPU were machined according to ASTM D638-14, ASTM D1621-10, ASTM D790-10, and ASTM D1622/D1622M-14 to determine the tensile, compressive, flexural, and density properties of both materials, respectively (ASTM Standard D, 1621-10, 2010; ASTM Standard D, 1621-10/D, 1622M-14, 2014; ASTM Standard, D638-14, 2014; ASTM Standard, D790-10, 2010). All tests were performed at room temperature in air.

Five tension test specimens with initial 50 mm gauge length (L_t) were machined from stock AC and HDPU. Average cross-sectional area (CSA_t) of the AC and HDPU tension test specimens were 78.5 ± 6.78 mm and 87.1 ± 1.74 mm (95% confidence interval (CI)), respectively. Each tension test specimen was clamped into a MTS Sintech 10/GL testing machine (MTS, Eden Prairie, MN) using self-aligning tension grips such that the distance between grips was 115 mm. A quasi-static displacement (5.0 mm/min) was applied to each specimen until failure, the moment of rupture of the test specimen. Force (F_t) and extension data (δ_t) were directly measured from the MTS testing system load cell and crosshead, respectively. Tensile stiffness (K_t) was calculated using linear regression to determine the slope within the linear region of the F_t vs δ_t curve, represented by Eq. (1). Elastic tensile modulus for the AC ($E_{t,AC}$) and HDPU ($E_{t,HDPU}$) were computed using Eq. (2).

$$K = \frac{F}{\delta} \tag{1}$$

$$E_t = K_t\frac{L_t}{CSA_t} \tag{2}$$

Five compression test specimens with initial height (h_c) 50.8 ± 0.026 mm and 25.2 ± 0.396 mm (95% CI) were machined from stock AC and HDPU, respectively. Average cross-sectional area (CSA_c) of the AC and HDPU compression test specimens were 162 ± 0.891 mm and 2580 ± 1.87 mm (95% CI), respectively. Each

compression test specimen was placed into a MTS Sintech 10/GL testing machine (MTS, Eden Prairie, MN) between compression platens. A quasi-static displacement (1.2 mm/min) was applied to each specimen until either a yield point was reached or until the specimen had been compressed approximately 13% of its original height, whichever occurred first. Force (F_c) and deflection data (δ_c) were directly measured from the MTS testing system load cell and crosshead, respectively. Compressive stiffness (K_c) was calculated using linear regression to determine the slope within the linear region of the F_c vs δ_c curve, represented by Eq. (1). Elastic compressive modulus for the AC ($E_{c,AC}$) and HDPU ($E_{c,HDPU}$) were computed using Eq. (3).

$$E_c = K_c \frac{h_c}{CSA_c} \tag{3}$$

Five bending test specimens were machined from stock AC and HDPU with initial height (h_b) 3.20 ± 0.020 mm and width (b_b) 12.7 ± 0.030 (95% CI). A standard four-point bend testing procedure was performed on each bending test specimen using a MTS Sintech 10/GL testing machine (MTS, Eden Prairie, MN) under quasi-static displacement (1.2 mm/min). The distances between the lower (L) and upper supports were 50.8 and 25.4 mm, respectively. The supports had radii of curvature of 2.5 mm at each point of contact with the bending test specimen. Each specimen was loaded until a maximum strain in the outer surface of the test specimen reached 0.05 mm/mm (at a measured crosshead displacement of approximately 4.89 mm) or at break, whichever occurred first. Force (F_b) and deflection data (δ_b) were directly measured from the MTS testing system load cell and crosshead, respectively. Bending stiffness (K_b) was calculated using linear regression to determine the slope within the linear region of the F_b vs δ_b curve, represented by Eq. (1). Elastic bending modulus for the AC ($E_{b,AC}$) and HDPU ($E_{b,HDPU}$) were computed using Euler-Bernoulli (EB) beam theory for prismatic, long beams in pure bending (Eq. (4)); where, a (= 12.7 mm) is the constant moment arm from the upper to the lower support, x (= a) is the position at which δ_b was measured, and I (= 34.6 ± 0.71 mm^4 (95% CI)) is the second moment of area about the bending axis (Eq. (5)).

$$E_b = \frac{a(3Lx - 3x^2 - a^2)K_b}{12I} \tag{4}$$

$$I = \frac{b_b h_b^3}{12} \tag{5}$$

The five machined bending test blanks of stock AC and five blocks of stock HDPU were used to determine the density of each material. The density (ρ) of the AC and HDPU were calculated using Eq. (6) where m is the average sample dry mass and V is the average sample volume.

$$\rho = \frac{m}{V} \tag{6}$$

2.3. Bone surrogate fabrication and evaluation

Conventional machine shop equipment (Eisen Milling Machine with Proto Trak EMX controller and a Sharp 1640 LV lathe) was used to fabricate three surrogates. A 0.50 mm corner rounding end mill was used to radius the shell edges along the length of each surrogate in order to enhance durability should the surrogate be dropped or mishandled overtime.

The surrogates were imaged using a Discovery CT750 HD computed tomography (CT) scanner (GE Healthcare, Little Chalfont, United Kingdom) with 0.625 mm cubic voxel size at 120 kV and 60 mA. Images were reconstructed using accompanying scanner software and imported as Digital Imaging and Communications in Medicine (DICOM) images into the medical image processing software Mimics 17.0 (Materialise, Ann Arbor, MI). The surrogates were segmented into volume masks of the individual shells and cores to determine the AC and HDPU average Hounsfield Unit (HU) densities.

The flexural rigidity of the fabricated surrogates about the x- (EI_x) and y-axis (EI_y) (Fig. 1) were calculated from the product of the

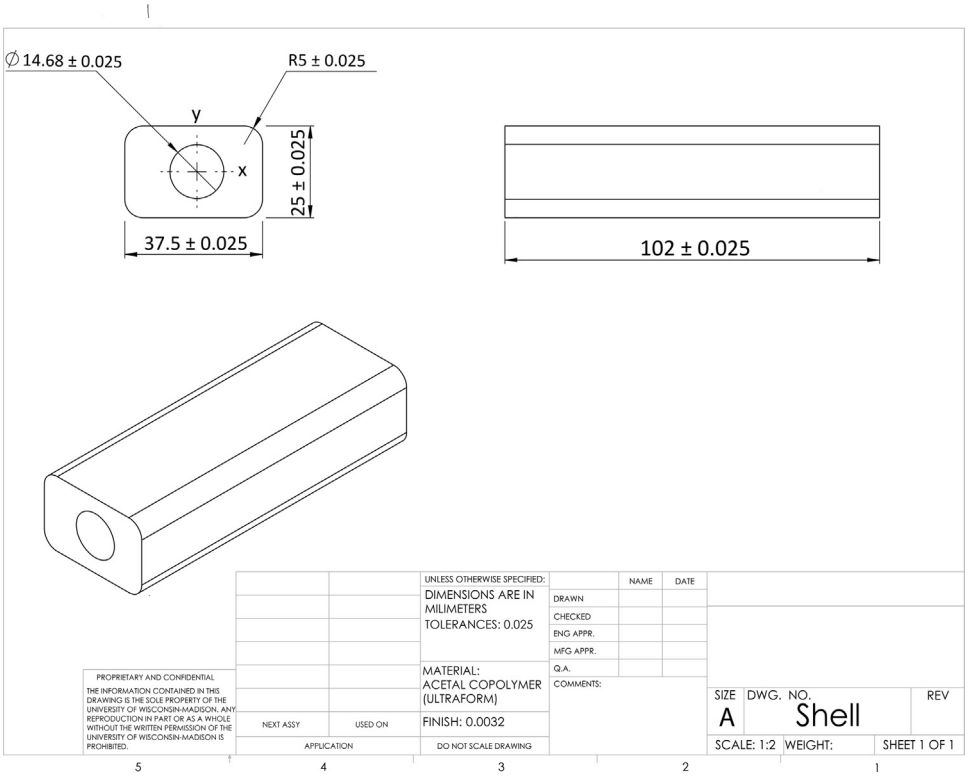

Fig. 1. Computer Aided Design (CAD) drawing of the final bone surrogate design with the locational transitional fit. Given dimensions are in mm. All design features were machined with a 0.025 mm tolerance and a finish of 0.0032 mm.

composite second moment of area about the respective bending axes and $E_{b,AC}$ (Eqs. (7) and (8), respectively).

$$EI_x = E_{b,AC}\left[\frac{wh^3}{12} + \left(\frac{E_{b,HDPU}}{E_{b,AC}} - 1\right)\left(\frac{\pi r^4}{4}\right)\right] \quad (7)$$

$$EI_y = E_{b,AC}\left[\frac{w^3h}{12} + \left(\frac{E_{b,HDPU}}{E_{b,AC}} - 1\right)\left(\frac{\pi r^4}{4}\right)\right] \quad (8)$$

The three fabricated surrogates underwent four-point bending tests using an MTS Sintech 10/GL testing machine (MTS, Eden Prairie, MN) with displacement rate of 5.0 mm/min. Each surrogate underwent three separate four-point bending tests. The distances between upper and lower supports were 12.7 mm (a) and 50.8 mm (L), respectively. The radii of curvature at each point of contact with the surrogates were 2.5 mm. The surrogates were loaded well below the surrogate yield strength. Force and displacement were directly measured from the MTS testing system load cell and crosshead, respectively. Effective flexural rigidity (EI_{eff}) of the surrogate was calculated using Euler-Bernoulli (EB) beam theory for prismatic, long beams in pure bending (Eq. (9)); where K_s is the bending stiffness of the surrogate, calculated from the four-point bending mechanical test force (F) and deflection (δ) data (Eq. (1)), and x (12.7 mm) is the position of the measured displacement. The Hertzian compression equation (Eq. (10)) was used to determine the theoretical local deformation, y, of the surrogate at the point of contact with the supports, where $\bar{F}$ is the applied force per until length, w is the length of contact (i.e. width of the final surrogate), D is the support diameter (0.5 mm), and ν_1, ν_2, E_1, and E_2 are the Poisson's ratios and elastic moduli of the steel support and AC shell, respectively (Puttock et al., 1969). The surfaces of the support and the surrogate were idealized as a cylinder and a plane, respectively. Adjusted effective flexural rigidity ($EI_{eff,adj}$) of the surrogate was calculated using Eq. (9) where K_s is the true bending stiffness of the surrogate, calculated from the four-point bending mechanical test force ($\bar{F}$) and the adjusted deflection data ($\delta_{adj} = \delta\text{-}2y$) (Eq. (1)).

$$EI_{eff} = \frac{a(3Lx - 3x^2 - a^2)K_s}{12} \quad (9)$$

$$y = \bar{F}\left(\frac{1-\nu_1}{\pi E_1} + \frac{1-\nu_2}{\pi E_2}\right)\left[1 + \ln\left\{\frac{8\left(\frac{w}{2}\right)^2}{\left(\frac{1-\nu_1}{\pi E_1} + \frac{1-\nu_2}{\pi E_2}\right)\bar{F}D}\right\}\right] \quad (10)$$

A one-way Analysis of Variance (ANOVA) was used to determine if any significant differences in $EI_{eff,adj}$ existed between the surrogates with different fits using Minitab® 15 (Minitab Inc., State College, Pennsylvania). Average $EI_{eff,adj}$ values and their 95% CIs estimated from the ANOVA models were plotted for each fit clearance or interference value.

3. Results and discussion

3.1. Materials testing

The results of the density measurements are presented in Table 1. The calculated density of the AC (1.40 g/cm^3) was well within the range of reported manufacturer and literature values for AC density (Range: 1.40–1.43 g/cm^3) (BASFSE, 2015; Osswald and Menges, 2003). The calculated density of the HDPU (0.724 g/cm^3) was greater than the reported range of literature values for Grade 40 HDPU density (Range: 0.577–0.705 g/cm^3) (ASTM Standard F, 1839-08, 2016).

The results of the tension, compression, and four-point bending materials testing are presented in Table 2. The AC and HDPU exhibited the greatest strength in bending (2850 ± 82.0 MPa (95% CI) and 596 ± 49.1 MPa (95% CI), respectively) and the lowest strength in tension (384 ± 22.6 MPa (95% CI) and 212 ± 10.1 MPa (95% CI), respectively). The calculated bending moduli for the AC (2850 MPa) was similar to the AC flexural moduli (2450 MPa) reported by the manufacturer (BASFSE, 2015). In contrast, the tensile modulus of the AC (384 MPa) was well below manufacturer and literature reported values (2600 MPa) (BASFSE, 2015; Osswald and Menges, 2003). The calculated compressive modulus of the HDPU (342 MPa) was lower than the range of expected values for Grade 40 HDPU (Range: 603–941 MPa) (ASTM Standard F, 1839–08, 2016; Calvert et al., 2010). Rather, the calculated compressive modulus of the HDPU fell within the range of expected values for Grade 25 HDPU (Range: 254–390 MPa), which has a much lower reported density (Range: 0.361–0.441 g/cm^3). No direct values were found within the literature for the tensile modulus of polyurethane foam with densities greater than 0.420 g/cm^3 (Goods et al., 1998; Marsavina et al., 2013). No literature values were found for compressive modulus of AC or for flexural modulus of HDPU. The ratio of compressive strength to tensile strength for the AC and HDPU were roughly 6.0 and 1.6, respectively.

Displacement rates used in the materials testing were quasi-static (1.2–5 mm/min) since the surrogate was designed to be tested under similar conditions. The standard for determining tensile properties of plastics prescribes a range of displacement rates, e.g. 5, 50, and 500 mm/min, some much faster than the quasi-static conditions used in this study (ASTM Standard, D638-14, 2014). The tensile test displacement rate of 5 mm/min was selected based on the requirement that the lowest speed, which produces rupture in 0.5–5.0 min, should be used (ASTM Standard, D638-14, 2014). Failure of all of the HDPU and AC tension specimens occurred within 0.5–1.5 min and 5.0–6.0 min, respectively. Displacement of the specimens was tracked using the position of the crosshead. Therefore, the underestimation of the AC tensile modulus may have been a result of the specimens slipping within the tension grips. The compression test displacement rate was nearly half that of the recommended rate (2.5 ± 0.25 mm/min) (ASTM Standard D, 1621-10, 2010). Since HDPU exhibits viscoelastic behavior, the difference in strain rate may have contributed to the underestimation of the HDPU compressive modulus. Further, age of the stock HDPU may have contributed to the elevated density and reduced compressive properties.

Table 1
Summary of physical density measurement results.

Specimen	Acetyl copolymer (AC) ρ_{AC} (g/cm^3)	High density polyurethane foam (HDPU) ρ_{HDPU} (g/cm^3)
1	1.40	0.723
2	1.40	0.730
3	1.39	0.723
4	1.40	0.722
5	1.42	0.723
Average	1.40	0.724
95% CI	0.008	0.003

Table 2
Summary of the tensile, compressive, and four-point bending materials testing results.

Specimen	Acetyl copolymer (AC)			High density polyurethane foam (HDPU)		
	$E_{t,AC}$ (MPa)	$E_{c,AC}$ (MPa)	$E_{b,AC}$ (MPa)	$E_{t,HDPU}$ (MPa)	$E_{c,HDPU}$ (MPa)	$E_{b,HDPU}$ (MPa)
1	414	2390	2740	192	350	527
2	318	2190	2770	212	348	649
3	348	2180	2920	219	333	646
4	384	2300	2880	218	339	548
5	403	2430	2950	218	342	610
Average	384	2300	2850	212	342	596
95% CI	22.6	115	82.0	10.1	5.68	49.1

3.2. Bone surrogate fabrication

The outer dimensions of the surrogate shells were milled from extruded stock AC with 32.0 mm × 38.5 mm × 102 mm dimensions. The w and h of the shells were machined to 37.5 ± 0.025 mm and 25 ± 0.025 mm, respectively, with 3.2 µm surface finish using a 10 mm end mill (Fig. 1). In order to achieve the goal flexural rigidity, an ideal radius of the central hole was calculated using Eq. (11) and the dimensions of the outer shell ($R = 5.91$ mm).

$$R = \sqrt{\frac{EI_{Goal} - E_{b,AC}\left(\frac{wh^3}{12}\right)}{\frac{\pi}{4}(E_{b,HDPU} - E_{b,AC})}} \tag{11}$$

For ease of machining, the central hole in the AC shells was drilled and then bored to a diameter of 7.34 ± 0.025 mm (Fig. 1). The diameter of each core was turned down from stock HDPU and machined to 14.478 ± 0.025 mm, 14.681 ± 0.025 mm, and 15.113 ± 0.025 mm in order to fabricate surrogates with a locational clearance (H7/h6), locational transitional fit (N7/h6), or medium drive (S7/h6) fit, respectively. All machining tolerances and fits were selected using the ASM Handbook and the ISO System of Limits and Fits (ASTM International Handbook Committee, 1999; ISO 286-2, 2012). The HDPU cores were pressed into the AC shells with the help of an aluminum sleeve, which was able to slide on and off the HDPU cores with little effort (diagram in Fig. 2). The sleeve prevented any local swelling of the HDPU cores near the opening, i.e. insertion point, of the shells. No lubricants or adhesives were applied at the interface of the core and shell to aid in assembly. A complete surrogate is shown in Fig. 3 adjacent to an excised adult porcine femur.

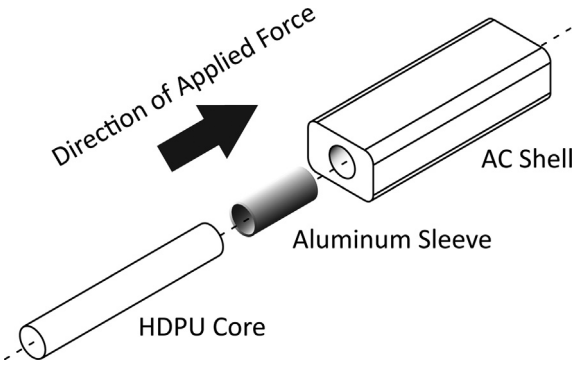

Fig. 2. Schematic depicting the assembly of the bone surrogate.

Fig. 3. Photo of a fabricated surrogate (Right) adjacent to an excised adult porcine femur (Left).

3.3. Bone surrogate evaluation

The CT densities for the bone surrogate materials were $HU_{AC,avg} = 297 \pm 85.4$ HU and $HU_{HDPU,avg} = -295 \pm 64.2$ HU (95% CIs), for the AC and HDPU respectively. In comparing the HU densities to their physical densities, the following linear relationship was found:

$$\rho = (1.14e{-}3)HU + 1.06 \tag{12}$$

Using Eq. (12) with a HU for water of 0, the physical density of water would be estimated as 1.06 g/cm^3, 6% different than expected. Because of limitations of commercially available materials, the density range of the surrogate materials is lower than pig bone, 200–1800 HU (Aiyangar et al., 2010). The relatively low material densities were offset with increased section properties. Flexural rigidity of different animal models and disease states could be mimicked with modifications to the surrogate design including materials and section properties. For example, the shell thickness could be modified to represent cortical thinning and a lower Grade of HDPU could be selected for the core to represent endocortical trabecularization, both associated with aging and, in extreme cases, osteoporosis in humans.

Based on the final design of the surrogate EI was calculated about both the x- and y-axis (Fig. 1). Bending about the x-axis ($EI_x = 1.34 \times 10^8$ Nmm^2) was more compliant than bending about the y-axis ($EI_y = 3.08 \times 10^8$ Nmm^2). Both were similar to EI_{Goal}, 1–2 × 10^8 Nmm^2, defined in the PDS and based on reported values for a porcine femur. EI_x fell within the desired range of flexural rigidity, while EI_y was closer to reported values for human femur flexural rigidity with the anterior surface in tension (3.2–3.7 × 10^8 Nmm^2 (Cristofolini et al., 1996; Heiner, 2008)).

The maximum load applied to the surrogates was 6026 N. Based on this and the width of the surrogate, 37.5 mm, $\bar{F}$ was determined to be 80.35 N/mm. An elastic modulus of 200 GPa (E_1) and Poisson's ratio of 0.3 (ν_1) were used for the steel cylinder. The calculated $E_{c,AC}$ of 2300 MPa (E_2) and Poisson's ratio of 0.363 (ν_2), found within the literature (BASFSE, 2015; Osswald and Menges, 2003), were used for the AC plane. The total local deflection under the supports, $2y$, was calculated to be 0.21 mm, which was 30% of the crosshead displacement.

Under four-point bending EI_x ranged from 0.26 ± 0.012–0.27 ± 0.006 × 10^8 Nmm^2 for all three surrogates (Fig. 4). No significant differences were found in $EI_{eff,adj}$ between the surrogates with H7/h6, N7/h6, or S7/h6 fits ($p = 0.193$) (Fig. 4). The difference in EI_x between the mechanical testing results (≈ 0.27 x 10^8 Nmm^2) and analytical calculation (= 1.34 x 10^8 Nmm^2) is due to the assumptions of the Euler-Bernoulli equations. The lower support length

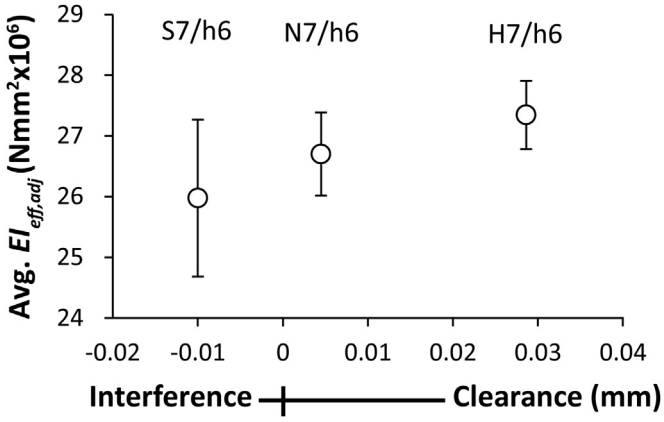

Fig. 4. Average adjusted effective flexural rigidity, $EI_{eff,adj}$, versus interference or clearance fit dimension, with 95% confidence interval (CIs) labeled. No significant difference was found in $EI_{eff,adj}$ between surrogates with the locational clearance (H7/h6), locational translational (N7/h6), or medium drive (S7/h6) fits.

to surrogate height ratio (2:1) is significantly smaller than required for negligible shear deformation (20:1) (Timoshenko, 1921).

4. Conclusion

Maintaining durability and CT compatibility while still achieving the desired stiffness proved to be major design challenges. Further, the results of the materials testing emphasize the importance of evaluating stock material prior to fabrication. Despite these challenges, the final design of the porcine bone surrogate presented in this study met all of the design requirements. The well-defined geometry and material properties of the surrogate enables relative electron density calibration of CT data in addition to cross-comparison of mechanical test and analysis results between research labs. Moreover, the design process detailed within this study can be used to generate surrogates of human or other common animal bones used in biomechanics research (i.e. mice, sheep, etc.).

Acknowledgments

The authors thank Alaa Ahmed and Chris Besaw for assisting with materials testing. Funding was provided by the Hilldale Undergraduate/Faculty Research Fellowship, United States; the University of Wisconsin-Madison Graduate School, United States; and the Wisconsin Alumni Research Foundation (WARF), United States. The funders had no role in study design, data collection and analysis, decision to publish, or preparation of the manuscript.

Declarations of interest

None.

References

Aiyangar, A.K., Au, A.G., Crenshaw, T.D., Ploeg, H.-L., 2010. Recovery of bone strength in young pigs from an induced short-term dietary calcium deficit followed by a calcium replete diet. Med. Eng. Phys. 32, 1116–1123. https://doi.org/10.1016/j.medengphy.2010.08.001.

ASTM International Handbook Committee, 1999. Machining, 16th ed. ASTM Handbook, Ohio.

ASTM Standard D1621-10, 2010. Standard Test Method for Compressive Properties of Rigid Cellular Plastics. ASTM International, West Conshohocken, PA. https://doi.org/10.1520/D1621-10.

ASTM Standard D1622/D1622M-14, 2014. Standard Test Method for Apparent Density of Rigid Cellular Plastics. ASTM International, West Conshohocken, PA. https://doi.org/10.1520/D1622_D1622M-14.

ASTM Standard D638-14, 2014. Standard Test Method for Tensile Properties of Plastics. ASTM International, West Conshohocken, PA. https://doi.org/10.1520/D0638-14.

ASTM Standard D790-10, 2010. Standard Test Methods for Flexural Properties of Unreinforced and Reinforced Plastics and Electrical Insulating Materials. ASTM International, West Conshohocken, PA. https://doi.org/10.1520/D0790-10.

ASTM Standard F1839-08, 2016. Standard Specification for Rigid Polyurethane Foam for Use as a Standard Material for Testing Orthopedic Devices and Instruments. ASTM International, West Conshohocken, PA. https://doi.org/10.1520/F1839-08R16.

BASFSE, 2015. Ultraform(R) H2320 006 - Product Datasheet. Ludwigshafen, Germany.

Bramer, J.A.M., Barentsen, R.H., Vd Elst, M., De Lange, E.S.M., Patka, P., Haarman, H.J.T.M., 1998. Representative assessment of long bone shaft biomechanical properties: an optimized testing method. J. Biomech. 31, 741–745. https://doi.org/10.1016/S0021-9290(98)00101-8.

Calvert, K.L., Trumble, K.P., Webster, T.J., Kirkpatrik, L.A., 2010. Characterization of commercial rigid polyurethane foams used as bone analogs for implant testing. J. Mater. Sci. Mater. Med. 21, 1453–1461. https://doi.org/10.1007/s10856-010-4024-6.

Crenshaw, T.D., Peo, E.R., Lewis, A.J., Moser, B.D., Olson, D., 1981. Influence of age, sex, and calcium and phosphorus levels on the mechanical properties of various bones in swine. J. Anim. Sci. 52, 1319–1329.

Cristofolini, L., Viceconti, M., Cappello, A., Toni, A., 1996. Mechanical Validation of Whole Bone Composite Femur Models. J. Biomech. 29, 525–535.

Decker, S., Reifenrath, J., Omar, M., Krettek, C., Müller, C.W., 2014. Non-osteotomy and osteotomy large animal fracture models in orthopedic trauma research. Orthop. Rev. 6. https://doi.org/10.4081/or.2014.5575.

Dias, I.R., Camassa, J.A., Bordelo, J.A., Babo, P.S., Viegas, C.A., Dourado, N., Reis, R.L., Gomes, M.E., 2018. Preclinical and translational studies in small ruminants (sheep and goat) as models for osteoporosis research. Curr. Osteoporos. Rep. 16, 182–197. https://doi.org/10.1007/s11914-018-0431-2.

Goods, S.H., Neuschwanger, C.L., Henderson, C.C., Skala, D.M., 1998. Mechanical properties of CRETE, a polyurethane foam. J. Appl. Polym. Sci. 68, 1045–1055. https://doi.org/10.1002/(SICI)1097-4628(19980516)68:7<1045::AID-APP2>3.0.CO;2-F.

Heiner, A.D., 2008. Structural properties of fourth-generation composite femurs and tibias. J. Biomech. 41, 3282–3284. https://doi.org/10.1016/j.jbiomech.2008.08.013.

Heiss, C., Böcker, W., Daghma, D.E.S., Khassawna, T. El, 2017. A new clinically relevant T-score standard to interpret bone status in a sheep model pp. 326–335. ⟨https://doi.org/10.12659/MSMBR.905561⟩.

ISO 286-2, 2012. Geometrical product specifications (GPS) - ISO code system for tolerances on linear sizes - Part 2: Tables of standard tolerance classes and limit deviations for holes and shafts.

Marsavina, L., Linul, E., Viovoni, T., Sadowski, T., 2013. A comparison between dynamic and static fracture toughness of polyurethane foams. Polym. Test. 32, 673–680. https://doi.org/10.1016/J.POLYMERTESTING.2013.03.013.

Martini, L., Fini, M., Giavaresi, G., Giardino, R., 2001. Sheep model in orthopedic research: a literature review. Comp. Med. 51, 292–299. https://doi.org/10.1080/026404100750017832.

Osswald, T.A., Menges, G., 2003. Materials Science of Polymers for Engineers, 2nd ed. Hanser Gardener Publications, Inc, Cincinnati, Ohio.

Pearce, A.I., Richards, R.G., Milz, S., Schneider, E., Pearce, S.G., 2007. Animal models for implant biomaterial research in bone: a review. Eur. Cells Mater. 13, 1–10.

Puttock, M., Thwaite, E., National Standards Labratory (Australia), 1969. Elastic Compression of Spheres and Cylinders at Point and Line Contact. Commonwealth Scientific and Industrial Research Organization, Melbourne, Australia.

Wright, N.C., Looker, A.C., Saag, K.G., Curtis, J.R., Delzell, E.S., Randall, S., Dawson-Hughes, B., 2014. The recent prevalence of osteoporosis and low bone mass in the United States based on bone mineral density at the femoral neck or lumbar spine. J. Bone Miner. Res. 29, 2520–2526. https://doi.org/10.1002/jbmr.2269.